

Supporting Information

Construction and characterization of YPet fusion strains. A construct containing the last 500 bp of *fliM*, followed by *yPet* and then 500 bp downstream of *fliM* containing the last 9 codons of FliM, was generated by overlap extension PCR (1) and cloned into pDS132 (2). This was sequenced and inserted into the *E. coli* RP437 chromosome by allelic exchange (3). Expression levels of FliM-YPet in both JPA945 and JPA954 strains were compared to FliM expression level in wild-type *E. coli* RP437 by western blot and found to agree within experimental error. Swarm plate assays showed only a small reduction in chemotaxis and motility (~75% of the wild-type swarm diameter). CheY^{D13K/Y106W} and CheY^{D57A} were over-expressed from pIND4 (4) in the $\Delta cheY$ strain.

Estimating the total content of FliM-YPet per cell. The average fluorescence intensity observed per pixel $I_m(x_0, y_0, z_0)$ due to the diffusive cytoplasmic component of FliM-YPet (following subtraction of autofluorescence and instrumental background) at an arbitrary point (x_0, y_0, z_0) was modeled as a 3D convolution integral of the point spread function $P(x, y, z)$ of a single YPet molecule with the spatial distribution function for number density of YPet in the cell $dN/dV(x, y, z)$, multiplied by the normalized local fluorescence excitation intensity function $L(x, y, z)$ over the 3D cellular volume:

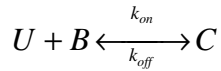
$$\begin{aligned} I_m(x_0, y_0, z_0) dA &= I_{YPet} \frac{dN}{dV} \otimes P \otimes L = I_{YPet} \iiint_{cell} \frac{dN}{dV} P(x - x_0, y - y_0, z - z_0) L(x, y, z) dx dy dz \\ &= n I_{YPet} \iiint_{cell} P(x - x_0, y - y_0, z - z_0) \exp(-z/d) dx dy dz \\ &\equiv n I_{YPet} S \end{aligned}$$

P was estimated from an earlier investigation (5) which generated z -stack images for 20 nm diameter yellow fluorescent beads (Molecular Probes) immobilized to the coverslip surface. The integral limits were defined by the spatial boundaries of the cell body in x , y , z , approximating the cell as a cylinder of length $2\text{ }\mu\text{m}$ and diameter $1\text{ }\mu\text{m}$ with hemispherical caps. The number density of YPet molecules, n , was approximated as constant throughout the cell. I_{YPet} is the unitary step size equivalent to the total summed intensity due to a single YPet molecule excited at the origin (i.e. when $L=1$), taken as $\sim 1,300$ counts on our camera detector (Fig. S2). The function L reflects the spatial distribution of the normalized fluorescence excitation field (here the TIRF evanescent field). Here d is the depth of penetration of the evanescent field which we measure using the method of ref. 5 as being $110 \pm 10\text{ nm}$. We assumed that the primary functional dependence in L is on z and not x or y (the length of a typical cell is small compared to the lateral width of the TIRF excitation field). In addition, the cell was assumed to be offset $\sim 50\text{ nm}$ from the coverslip surface due to the presence of the flagellar stub following truncation, as indicated previously (6). The pixel area dA at the sample plane is $50\text{ nm} \times 50\text{ nm}$. The integral S was estimated numerically using values of x_0 and y_0 over a range $\pm 2\text{ }\mu\text{m}$ centred on the model cell.

For the FliM-YPet strain we measured experimentally $I_m = 1450 \pm 200$ counts per pixel. Optimizing the value of S to fit this mean level of fluorescence intensity indicated $S = 29.6 \pm 5.2$ (Fig. S1). This implied a value of $n = 0.038 \pm 0.010$ YPet molecules per $50 \times 50 \times 50\text{ nm}$ voxel. We estimate that the average volume of a FliM-YPet (wt) strain cell was $16,800 \pm 6,300$ voxels. This indicates the total mean number of FliM-YPet in the cytoplasm is 630 ± 290 molecules per cell.

Cells photobleached for 10 s or more using epifluorescence illumination, in the presence of chloramphenicol to block protein synthesis, showed less than 1% fluorescence recovery after 20 min, indicating maturation of YPet chromophores was negligible on the time scale of our experiments.

Simulating turnover. Following previous studies (7–12), we modelled FliM turnover using a kinetic model describing reactions between diffusive FliM-YPet in the cytoplasm and the C-ring in a membrane-integrated flagellar motor:



U is the unbound population of photoactive FliM-YPet in the cell cytoplasm, B the FliM binding sites on a C-ring and C the bound population of photoactive FliM-YPet. The system contains particles described by reaction-diffusion kinetics (7–10).

$$\begin{aligned} \frac{\partial u}{\partial t} &= D \nabla_r^2 u - k_{on}^* u + k_{off} c, \\ \frac{\partial c}{\partial t} &= k_{on}^* u - k_{off} c \end{aligned}$$

Here \mathbf{r} is the position vector. This assumes a population of FliM bound to a flagellar motor C-ring, c , which is immobile, whereas free FliM-YPet, u , diffuses throughout the cell cytoplasm. We assume that the concentration of free binding sites B remains at a pseudo-equilibrium value B_{eq} throughout, implying a pseudo-first order reaction constant, $k_{on}^* = k_{on} B_{eq}$. The boundary conditions are Neumann zero flux, enforcing conservation of total mass. Immediately post-bleach ($t = 0$) the variables $u(t = 0, \mathbf{r})$ and $c(t = 0, \mathbf{r})$ are defined according to the experimental bleaching profile.

With simplifications, analytical solutions to the governing PDEs are obtainable (7, 11, 12). However, more complex diffusion-coupled systems with non-trivial domain geometry or lack of symmetry result in higher spatial dimensionality of the variables u and c and require numerical schemes to simulate the reaction-diffusion process, as was the case here. Simulation was employed similar to the methodology as reported previously for a reaction-diffusion system confined to the two-dimensional bacterial cell membrane (6) but here incorporating full 3D diffusion in the cell cytoplasm. The input parameters included in the algorithm were:

D = Diffusion coefficient

k_{on}, k_{off} = Kinetic rate parameters

B_{tot} = Total number of binding sites per motor complex

B_{nd} = Number of non-dynamic FliM attached to a motor complex

r_c = Capture radius of motor complex

σ = Spatial bleach width

t_p = Bleach pulse duration

A = Bleach magnitude

Ω = Analytic definition of the domain geometry

Δt = Simulation timestep

T = Total simulation time

The simulations were discrete and probabilistic, using a simple form of Brownian dynamics (13) at the molecular level. We assumed a realistic geometry of an *E. coli* cell, namely a cylinder capped at both ends with two hemispheres with a total length along the

long axis of 3 μm and common radius 0.5 μm (6). Using a diffusion-to-capture approach (14), C-rings were modeled as fixed capture zones mounted at positions on the cell membrane chosen to correspond closely with the experimentally observed positions of fluorescent foci, with a diameter of 50 nm as suggested by cryo-electron microscopy of the flagellar motor (15–17). Single FliM-YPet molecules were modeled as non-interacting point particles undergoing a Brownian random walk within the cytoplasm. The system was initialized with a simulated FRAP bleach pulse of duration $t_p = 300$ ms, focused typically close to the cell pole as was the case experimentally.

The bleach pulse had a characteristic Gaussian width σ and amplitude A , calculated from experimental bleaching data (see “Estimating diffusion coefficient” in *SI text*). We assumed a total of ~ 630 molecules of FliM-YPet per cell. For the motor bound component we ran simulations over a range of 14-30 dynamic molecules per motor. Best fits were obtained using ~ 20 dynamic FliM-YPet per motor with the remaining ~ 10 were static throughout in order to match observed asymptotic FRAP and FLIP levels (see “Estimating the non-dynamic fraction of FliM at the motor” in *SI text*).

Experimentally we estimate there were ~ 24 FliM-YPet complexes integrated into the membrane per cell. This corresponds to a mean separation of >1 μm which is very large compared to the diameter of the capture zone, thus the presence of additional complexes does not perturb the kinetics of the system in any significant way and we ignored these effects.

The fluorescence state of each FliM-YPet molecule was modeled as a binary system (either fluorescent or dark due to irreversible photobleaching) and the status of each molecule following the initial bleach was stored in memory. The simulations

modeled a continuous time reaction-diffusion system by sampling the system at sufficiently short discrete time steps as described by Andrews and Bray (18), here typically 0.1 ms.

The output of the simulation was designed to match the imaging data produced from a real FRAP experiment, namely the intensity at the motor due to protein turnover. Since the method is stochastic, the simulated data produced from a single iteration are noisy and many iterations are required to acquire a sufficiently smooth (averaged) FRAP curve (Fig. S2). In general for each set of parameters ~ 20 iterations minimized the simulation noise to a level smaller than the observed experimental error of the mean FRAP traces.

Due to the computational demands of the algorithm it was not possible to search through the entire parameter space for a complete parameter optimization. However, it has been suggested by Zadeh *et al.* that the problem of parameter optimization over the two kinetic parameters and the diffusion coefficient is not well-posed and there is no unique best-fitting set of these parameters (19). We therefore minimized the parameter search to include only the rate constants, constraining the other parameters to values determined by other means (see other sections herein for estimation methods).

A plot of the experimental FRAP data with overlaid simulation output for comparison is shown (Fig. S3). Following simulation with several different values for rate constants, we observed that most of the experimental data was found between simulations curves for k_{off} in the range 0.01-0.02 s⁻¹ and k_{on} set to an arbitrarily high value (in our case in excess of 10¹⁰ s⁻¹) imposing that the protein molecules react instantly upon collision with their complimentary binding site (6). We then used linear interpolation

between two bounding simulation traces of different k_{off} value for all mean experimental FRAP time points, which indicated a mean effective dwell time $\tau \sim 1/k_{off}$ for a single dynamic FliM-YPet protein molecule on the C-ring of ~ 40 s (s.d. error $\sim 70\%$).

Estimating diffusion coefficient. In a typical FRAP experiment it is often assumed that the bleach pulse is rapid compared with the timescale for diffusion in the sample. This is valid in the case of slowly diffusing fluorophores bleached with a short duration laser pulse. An example of is diffusion of fluorescent fusion proteins in a cell membrane where typically the diffusion constant is of the order of $\sim 0.01 \mu\text{m}^2 \text{s}^{-1}$ (5, 20). In the case of cytoplasmic diffusion however, particles diffuse several orders of magnitude faster (21, 22), typically $\sim 10 \mu\text{m}^2 \text{s}^{-1}$. Here the assumption of an instantaneous bleach pulse is not justified, since even a short pulse is on the order of 10-100ms. From simple Brownian diffusion theory the characteristic distance for a particle diffusing at $D \sim 10 \mu\text{m}^2 \text{s}^{-1}$ during a 100ms pulse t is $\sim (6Dt)^{1/2}$ or $\sim 2.5 \mu\text{m}$, comparable to the length of an *E. coli* bacterium, and substantially greater than typical bleach spot radii used in such experiments which is often $\sim 0.5 \mu\text{m}$. Hence many more fluorophores will travel through the bleach spot during a finite length bleach pulse than during a theoretical infinitely short pulse.

Due to the rapid nature of diffusion of FliM-YPet cytoplasmic component, it is technically non-trivial to image the recovery of fluorescence within the cytoplasm directly, as this is essentially complete before the first post-bleach time point is taken following FRAP. However, measurement of the pre- and post-bleach intensity at motor complexes, and asymptotic fluorescence recovery (FRAP) and loss (FLIP) values allows inference of the proportion of the bound and cytoplasmic fluorophore population which is

bleached during the initial laser pulse. The limiting normalized intensity values required are $I_{frap,(pre)}$, $I_{frap,(t=0)}$, $I_{flip,(pre)}$ and $I_{flip,(t=0)}$; based on these values one can calculate the proportion of bound protein units which exhibit dynamic turnover on the time scale of the experiment. In a similar manner it is possible to ascertain the fraction of free cytoplasmic components which remain photoactive post-bleach, f .

We assume photobleaching is a probabilistic Poisson process with decay rate of decay determined by the laser power. In the case of FRAP experiments, the laser power is modelled as a Gaussian in the xy focal plane. For a static fluorophore such as those bound to the motor complex, the time dependence of the concentration is:

$$\frac{\partial u}{\partial t} = -ku$$

where $u = u(t, x, y, z)$ is the concentration of active fluorophore and k is a rate constant describing the photobleaching process, giving a simple exponential solution for a continuum model. We assume that the value of the rate constant is directly proportional to the power of the laser at that spot. Our experimental protocol here allows us to calculate k at two distinct points in a bacterial cell, namely the FRAP and FLIP centers, as fluorophores at these two locations are static over the duration of the bleach pulse $t_p = 300$ ms. Considering the normalized intensity $I = I_{frap,(t=0)}$ and $t=300$ ms we deduce:

$$k = \frac{-\ln(1 - I_{t=0})}{t_p} \quad (1)$$

This is proportional to the laser intensity function G . This takes the form:

$$k \propto G(x, y) = A \exp\left(\frac{(x - x_b)^2 + (y - y_b)^2}{2\sigma^2}\right) \quad (2)$$

A is a constant expressing bleach magnitude, (x_b, y_b) are the coordinates of the bleach pulse focus and σ is the width of the pulse. The bleach focus is typically near to the cell pole and is denoted the origin of the coordinate system for simplicity, hence $x_b = y_b = 0$. Knowledge of the ratio of two spatially distinct values of the bleaching constant k allows inference of the bleach width by equating equations (1) and (2):

$$\begin{aligned} \frac{k_{frap}}{k_{flip}} &= \frac{G(x_{frap}, y_{frap})}{G(x_{flip}, y_{flip})} \\ &= \frac{\ln(1 - I_{frap, (t=0)})}{\ln(1 - I_{flip, (t=0)})} \\ &= \exp\left(\frac{-r_{frap}^2 + r_{flip}^2}{2\sigma^2}\right) \end{aligned}$$

where r_{frap} indicates the position vector of the FRAP region in the xy plane relative to the origin (the bleach focus). We solve for σ and A by a simple rearrangement and substitution. The experimental data and calculated constants are summarized below:

$$t_p = 0.3 \text{ s}$$

$$I_{frap, (t=0)} = 0.11$$

$$I_{flip, (t=0)} = 0.97$$

$$r_{frap} = (0, 0, 0.8) \mu\text{m}$$

$$r_{flip} = (0, 0, 2.8) \mu\text{m}$$

$$f=0.55$$

$$\sigma = 0.92 \mu\text{m}$$

$$A = 10.77 \text{ s}^{-1}$$

For simulations of diffusion during a photobleaching pulse a continuum model exists in the form of a partial differential equation (PDE) in terms of $u = u(t, x, y, z)$ (for a 3D domain such as the cell geometry under consideration here):

$$\frac{\partial u}{\partial t} = -D\nabla_r^2 u - A \exp\left(\frac{-(x^2 + y^2)}{2\sigma^2}\right) u \quad (3)$$

The first term corresponds to Brownian motion and the second is the Gaussian bleaching term, which is only dependent on the position in the xy plane. Zero flux Neumann boundary conditions ensure that the fluorescence is contained within the domain. The model domain is designed to mimic the shape of an *E. coli* cell and comprises a cylinder capped at either end with hemispheres (see “Simulating turnover” in *SI text*). A simple analytic solution of the governing PDE is not, to the best of our knowledge, obtainable on a complex domain thus we explored numerical solutions. We used a Monte Carlo algorithm, in a similar fashion to that used to simulate the FRAP itself. The procedure includes diffusion of discrete fluorescent molecules with probabilistic bleaching according to the laser intensity at their positions in the cell. To validate the model, the expected photobleaching was also calculated for a static diffusion scenario by numerical integration of the Gaussian bleaching function over the cell domain using the Matlab function *triplequad*. Figure S4 shows the effect of varying the diffusion coefficient in these simulations. These simulations indicate a value of $D = 7 \pm 5 \mu\text{m}^2 \text{s}^{-1}$ to best fit the observed experimental cytoplasmic bleached fraction $f \approx 0.55$. These results illustrate that with a very short laser pulse there is relatively little difference to the final bleached fraction – this is intuitively reasonable since large differences in bleached fraction will only be noticeable if the duration of the pulse is large enough to allow a significant

fraction of cytoplasmic FliM-YPet to diffuse through the laser focal waist. So, it is unsurprising that the curves are very similar for short duration pulses. For larger duration pulses the simulation curves do show clear deviation from each other. However, what they also indicate is that this relative deviation gets less for increasing increments of diffusion coefficient – this is also intuitively reasonable since a value of diffusion coefficient which increases the root mean squared displacement during the laser pulse much beyond the width of the laser pulse does not therefore result in any additional bleaching effect.

Estimating the non-dynamic fraction of FliM at the motor. Figure S5 illustrates idealized FRAP and FLIP traces both normalized for intensity relative to pre-bleach intensity levels, for which a focused laser bleach is applied at time zero (assuming a typically comparatively small correction for photobleaching at subsequent post-bleach observation time points). Generally, a fluorescent spot complex of FliM-YPet within the original laser spot bleach zone will have a small but non-zero fluorescence intensity following the bleach (level β), and similarly a fluorescent spot complex outside the laser focus will have a normalized intensity slightly less than 1 (level γ) since the laser focus does not have sharp boundaries but is a continuum. Here we denote:

S = total stoichiometry of the FliM-YPet complex,

I_1 = unitary intensity of a single photoactive YPet molecule,

α = dynamic fraction of the FliM-YPet complex,

$1-\alpha$ = non-dynamic fraction of the FliM-YPet complex,

f = average fraction of FliM-YPet photobleached in a single cell following a focused laser bleach,

$I_{FLIP}(t)$ = intensity of FLIP trace at time t following focused laser bleach ($t > 0$),

$I_{FRAP}(t)$ = intensity of FRAP trace at time t following focused laser bleach ($t > 0$).

At large time post-bleach of ~ 1000 s (pseudo-equilibrium) we assume that the proportion of bleached to unbleached FliM-YPet in the dynamic portion of the FliM-YPet complex is the same as that in the rest of the cell. Hence:

Total intensity of dynamic portion of complex at equilibrium = $(1-f)\alpha SI_1$

Total intensity of non-dynamic portion of complex following focused laser bleach for FRAP trace = $(1-\alpha)\beta SI_1$

Similarly, total intensity of non-dynamic portion of complex following focused laser bleach for FLIP trace = $(1-\alpha)\gamma SI_1$

Thus:

$$I_{FRAP}(\infty) = (1-f)\alpha SI_1 + (1-\alpha)\beta SI_1 = SI_1((1-f)\alpha + (1-\alpha)\beta)$$

$$I_{FLIP}(\infty) = (1-f)\alpha SI_1 + (1-\alpha)\gamma SI_1 = SI_1((1-f)\alpha + (1-\alpha)\gamma)$$

Rearranging:

$$\alpha = 1 - (I_{FLIP}(\infty) - I_{FRAP}(\infty)) / SI_1(\gamma - \beta)$$

Thus, the situation for which the FRAP and FLIP normalized intensity traces converge asymptotically at high time is indicative of turnover in a complex for which all the corresponding subunits are dynamic, as expected if the state has reached pseudo-equilibrium. The parameters β , γ , $I_{FRAP}(\infty)$ and $I_{FLIP}(\infty)$ were estimated using single exponential fits to the normalized photobleach-corrected intensity data for the mean curves for FRAP and FLIP datasets for the FliM-YPet (wt), the Δ CheY/FliM-

YPet/CheY^{D13K/Y106W} and the Δ CheY/ FliM-YPet/CheY^{D57A} strains, outlined in Table S1.

This indicates no statistical differences between the combined FRAP and FLIP mean data for the two strains, and a mean value of $\alpha = 0.64 \pm 0.21$. Assuming a mean stoichiometry of ~30 molecules per FliM-YPet complex this indicates the dynamic fraction consists of ~20 FliM-YPet molecules and the non-dynamic fraction ~10 FliM-YPet molecules. For the FliM-YPet (Δ CheY) strain a small increase (<5%) in the normalized FRAP intensity data could be observed after ~1000s post-bleach, which was fitted by a single exponential function, however the corresponding single exponential fit for the normalized FLIP trace was comparatively poor, but indicating a very small decrease in intensity of ~2%. This indicated that the corresponding $\alpha = 0.04 \pm 0.29$, consistent with no significant dynamic fraction within experimental error at least over the time scale of ~1000s of these experiments.

Performing FRAP and FLIP on putative assembly intermediate complexes.

To assess the turnover of putative assembly intermediate complexes we performed similar FRAP/FLIP analysis on fluorescent spots from immobilized cells with a stoichiometry within one s.d. of the mean of the peak at 18 molecules. These indicated no significant turnover within experimental error over the time scale of our observations of ~1,000 seconds and were of a comparable final intensity level to the Δ CheY strain (Fig. S6).

References

1. Wadhams GH, Warren AV, Martin AC, Armitage JP (2003) Targeting of two signal transduction pathways to different regions of the bacterial cell. *Mol. Microbiol.* 50:763-70.
2. Philippe N, Alcaraz JP, Coursange E, Geiselmann J, Schneider D (2004) Improvement of pCVD442, a suicide plasmid for gene allele exchange in bacteria. *Plasmid* 51:246-55.
3. Link AJ, Phillips D, Church GM (1997) Methods for generating precise deletions and insertions in the genome of wild-type *Escherichia coli*: application to open reading frame characterization. *J. Bacteriol.* 179:6228-37.
4. Ind AC, *et al.* (2009) An inducible expression plasmid for *Rhodobacter sphaeroides* and *Paracoccus denitrificans*. *Appl. Environ. Microbiol.* 75:6613-6615.
5. Lo CJ, Leake MC, Pilizota T, Berry RM (2007) Single-cell measurements of membrane potential, sodium-motive force and flagellar motor speed in *Escherichia coli*. *Biophys. J.* 93:294-302.
6. Leake MC, *et al.* (2006) Stoichiometry and turnover in single, functioning membrane protein complexes. *Nature* 443:355-358.
7. Sprague BL, Pego RL, Stavreva DA, McNally JG (2004) Analysis of binding reactions by fluorescence recovery after photobleaching. *Biophys. J.* 86:3473-3495.
8. Sprague BL, *et al.* (2006) Analysis of binding at a single spatially localized cluster of binding sites by fluorescence recovery after photobleaching. *Biophys. J.* 91:1169-1191.
9. Tsididis GD, Ripoll J (2008) Investigation of binding mechanisms of nuclear proteins using confocal scanning laser microscopy and FRAP. *J. Theor. Biol.*, 253:755-768.
10. Braga J, McNally JG, Carmo-Fonseca MA (2007) Reaction-diffusion model to study RNA motion by quantitative fluorescence recovery after photobleaching. *Biophys. J.*, 92:2694-2703.
11. Sprague B, McNally J (2005) FRAP analysis of binding: proper and fitting. *Trends Cell Biol.* 15:84-91.
12. Tsididis GD (2009) Quantitative interpretation of binding reactions of rapidly diffusing species using fluorescence recovery after photobleaching. *J. Microsc.* 233:384-390.

13. Cichocki B, Hinsen K (1990) Dynamic computer simulation of concentrated hard-sphere suspensions. 1. Simulation technique and mean square displacement data. *Physica A* 166:473-491.
14. Berg HC (1993) Random Walks in Biology. *Princeton University Press* Ed. 4.
15. Suzuki H, Yonekura K, Namba K (2004) Structure of the rotor of the bacterial flagellar motor revealed by electron cryomicroscopy and single-particle image analysis. *J. Mol. Biol.* 337:105-113.
16. Thomas DR, Morgan DG, DeRosier DJ (1999) Rotational symmetry of the C-ring and a mechanism for the flagellar rotary motor. *Proc. Natl. Acad. Sci. USA* 96:10134-10139.
17. Thomas DR, Francis NR, Xu C, DeRosier DJ (2006) The three-dimensional structure of the flagellar rotor from a clockwise-locked mutant of *Salmonella enterica* serovar Typhimurium. *J. Bacteriol.* 188:7039-7048.
18. Andrews SS, Bray D (2004) Stochastic simulation of chemical reactions with spatial resolution and single molecule detail. *Phys. Biol.* 1:137-151.
19. Zadeh KS, Elman HC, Montas HJ, Shirmohammadi, A (2007) A finite element model for protein transport in vivo. *BioMed. Eng. OnLine*, 10.1186/1475-925X-6-24, 6-24.
20. Leake MC *et al.* (2008) Variable stoichiometry of the TatA component of the twin-arginine protein transport system observed by in vivo single-molecule imaging. *Proc Natl Acad Sci USA* 105:15376-15381.
21. Lenn T, Leake MC, Mullineaux CW (2008) Clustering and dynamics of cytochrome bd-I complexes in the *Escherichia coli* plasma membrane in vivo. *Mol. Microbiol.* 70:1397-1407.
22. Segall JE, Ishihara A, Berg HC (1985) Chemotactic signaling in filamentous cells of *Escherichia coli*. *J. Bacteriol.* 161:51-59.

Figure S1. Fluorescence intensity per pixel (false-colour) due to diffusive component of FliM-YPet in the cytoplasm calculated using a 3D convolution model, displayed as (A), 3D contour plot, and (B), projection onto xy plane.

Figure S2. Single simulation iterations (grey) and an averaged curve from 20 iterations (red), with typical experimental FRAP data overlaid (blue).

Figure S3. Typical experimental FRAP data with overlaid simulated FRAP curves using different values for off-rate, k_{off} .

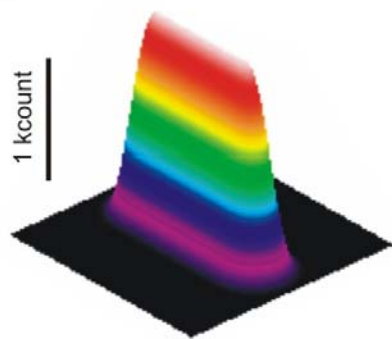
Figure S4. Dependence on extent of bleaching on the diffusion coefficient, D , for a bleach pulse of duration 300 ms centred at the cell pole for a cell of length 3 μm and radius 0.5 μm .

Figure S5. Idealized FRAP (red) and FLIP (blue) traces normalized with respect to pre-bleach levels, with an assumed non-dynamic population (solid lines) and with all components dynamics (dotted lines).

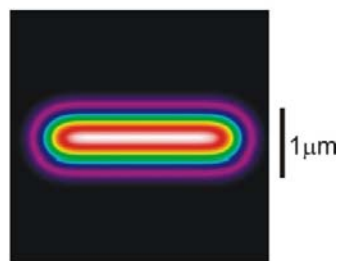
Figure S6. Mean FRAP (red) and FLIP (blue) traces (s.e.m. error bounds shown as dotted lines) for the FliM-YPet (wt) strain using immobilized cells and fluorescent spots whose estimated pre-bleach stoichiometry was within one s.d. of 18 molecules, 9 spots used for each mean trace.

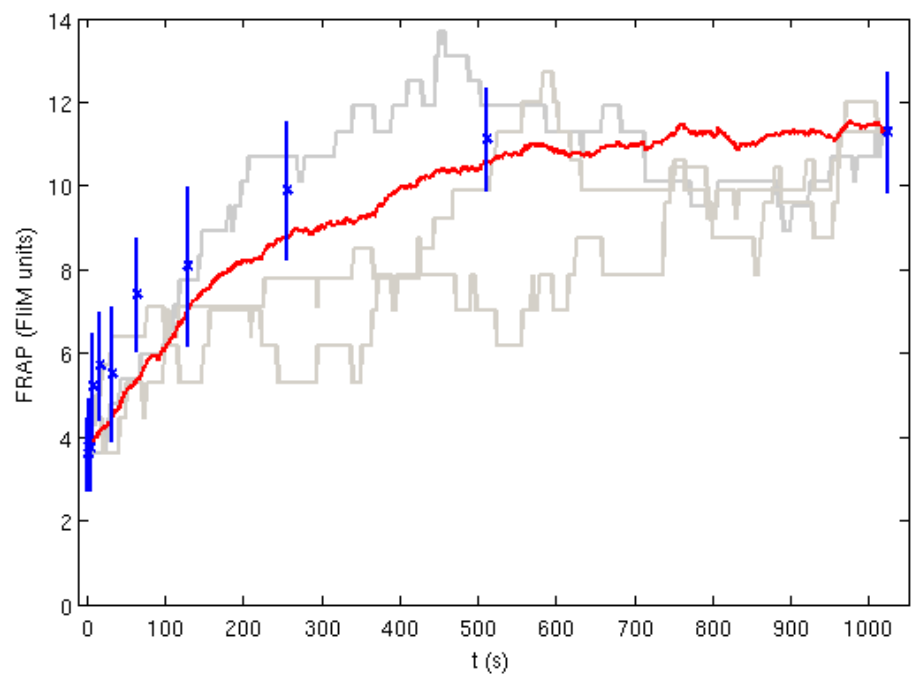
Table S1. Table for single exponential fit parameters [s.d.] to normalized turnover traces. The value of t_b is the mean photobleach time from FRAP and FLIP datasets combined.

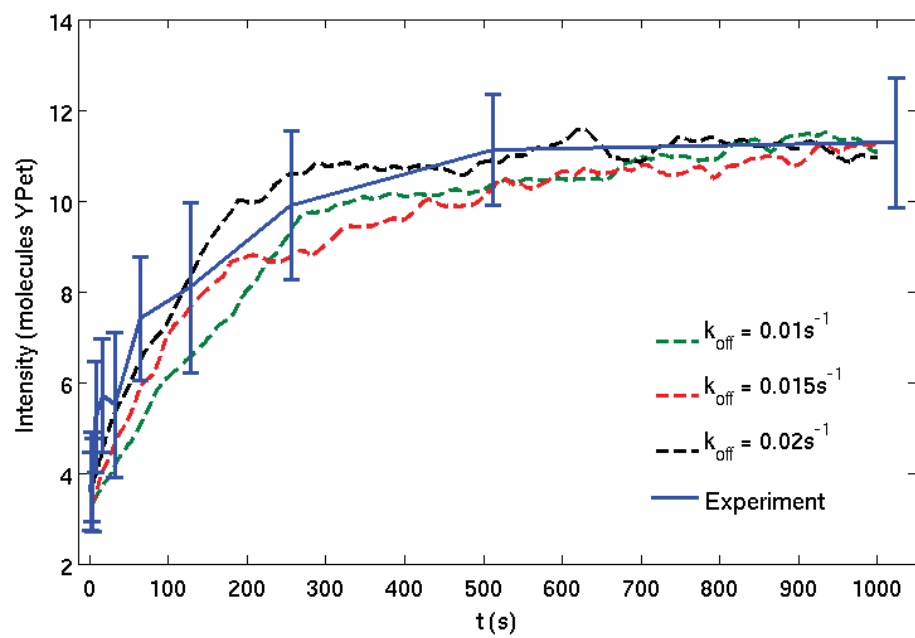
A

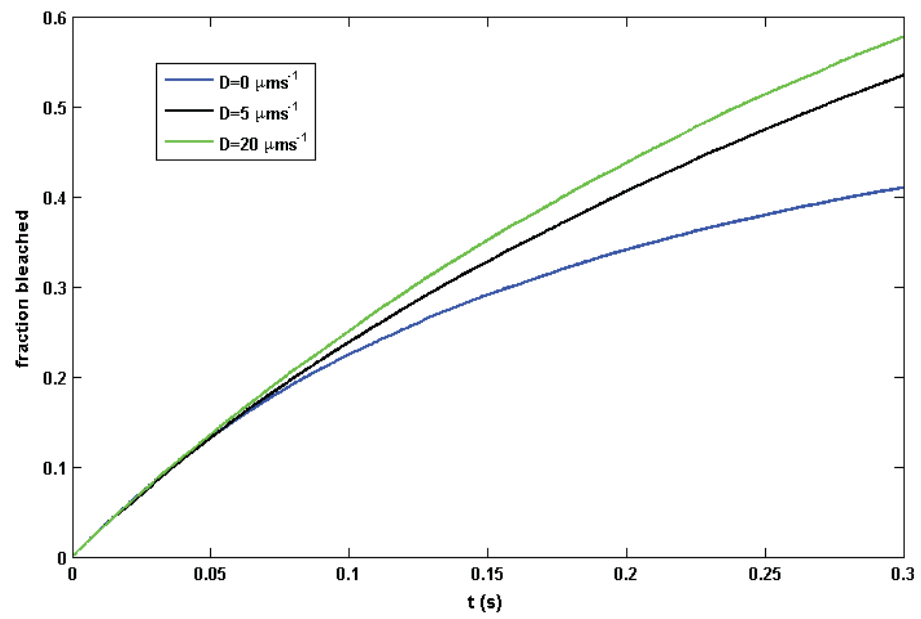


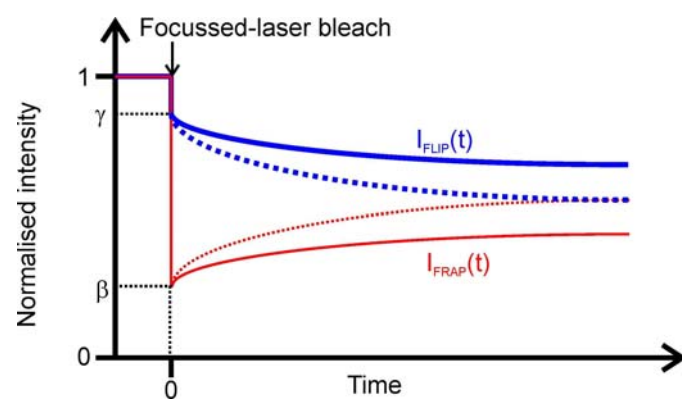
B

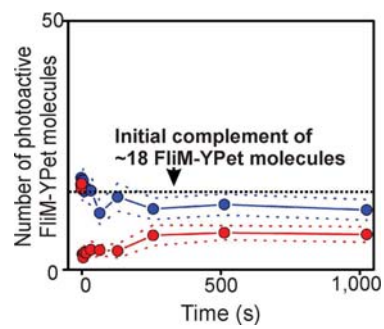












Strain	Normalized $I_{FRAP}(\infty)$	Normalized $I_{FLIP}(\infty)$	β	γ	t_b (s)	α
FliM-YPet (wt)	0.33	0.64	0.11	0.97	180	0.64
	[0.09]	[0.14]	[0.09]	[0.17]	[28]	[0.20]
FliM-YPet (Δ CheY)	0.14	0.99	0.11	1.00	390	0.04
	[0.04]	[0.20]	[0.03]	[0.15]	[205]	[0.29]
FliM-YPet(Δ CheY, CheY ^{D57A})	0.21	0.78	0.14	0.99	186	0.67
	[0.04]	[0.20]	[0.03]	[0.24]	[45]	[0.30]
FliM-YPet(Δ CheY, CheY ^{D13K/Y106W})	0.31	0.70	0.04	1.10	202	0.65
	[0.04]	[0.20]	[0.03]	[0.20]	[24]	[0.21]

Supplementary Movie 1. Brightfield movie of tethered FliM-YPet (wt) cell.

Supplementary Movie 2. TIRF and focused-laser bleach movie of the same cell of Supplementary Movie 1.

Supplementary Movie 3. Movie of same cell of Supplementary Movies 1,2 taken 10 min after focused laser bleach. Recovery of fluorescence intensity can be seen at the original bleached motor position.

